

Deep Multimodal Learning: Merging Sensory Data for Massive MIMO Channel Prediction

Yuwen Yang, Feifei Gao, Chengwen Xing, Jianping An and Ahmed Alkhateeb

Abstract

Existing work in intelligent communications has recently made preliminary attempts to utilize multi-source sensing information (MSI) to improve the system performance. However, the research on MSI aided intelligent communications has not yet explored how to integrate and fuse the multimodal sensory data, which motivates us to develop a systematic framework for wireless communications based on deep multimodal learning (DML). In this paper, we first present complete descriptions and heuristic understandings on the framework of DML based wireless communications, where core design choices are analyzed in the view of communications. Then, we develop several DML based architectures for channel prediction in massive multiple-input multiple-output (MIMO) systems that leverage various modality combinations and fusion levels. The case study of massive MIMO channel prediction offers an important example that can be followed in developing other DML based communication technologies. Simulations results demonstrate that the proposed DML framework can effectively exploit the constructive and complementary information of multimodal sensory data in various wireless communication scenarios.

Index Terms

Deep multimodal learning (DML), deep learning, wireless communications, channel prediction, massive MIMO

Y. Yang and F. Gao are with Institute for Artificial Intelligence Tsinghua University (THUAI), State Key Lab of Intelligent Technologies and Systems, Beijing National Research Center for Information Science and Technology (BNRist), Department of Automation, Tsinghua University, Beijing, 100084, P. R. China (email: yyw18@mails.tsinghua.edu.cn, feifeigao@ieee.org).

C. Xing and J. An are with the School of Information and Electronics, Beijing Institute of Technology, Beijing 100081, China (e-mail: chengwenxing@ieee.org; an@bit.edu.cn).

A. Alkhateeb is with the School of Electrical, Computer and Energy Engineering at Arizona State University, Tempe, AZ 85287, USA (e-mail: alkhateeb@asu.edu).

I. INTRODUCTION

To satisfy the demand of explosive wireless applications, e.g., diverse intelligent terminal access, autonomous driving, and Internet of Things, etc, the new generation of wireless communication systems are expected to handle massive data and meet the requirements of both high-reliability and low-latency. However, existing communication systems, which are basically designed based on conventional communication theories, exhibit several inherent limitations in meeting the aforementioned requirements, such as relying on accurate theoretical models, suffering from high complexity algorithms, and being restricted to block-structure communication protocols, etc [1]. Recently, intelligence communication has been recognized as a promising direction in future wireless communications. As a major branch of machine learning, deep learning (DL) has been applied in physical layer communications as a potential solution to deal with the massive data and the high complexity of wireless communication systems [2], [3]. By merging DL into existing communication systems, many remarkable progresses have been made in various applications such as channel estimation [4]–[11], data detection [12], [13], channel feedback [14]–[16], beamforming [17]–[20], and hybrid precoding [21], etc.

Compared with conventional communications that are based on statistics and information theories, DL based communications benefit from both the excellent learning capability of deep neural networks (DNNs) and the impressive computational throughput of parallel processing architectures. Moreover, DL does not require tractable mathematical models or high computational operations. Among these superiorities, the most advantageous aspect of DL is its ability to handle problems with imperfect models or without mathematical models. Interestingly, there exists out-of-band side-information in communication systems that can be utilized to improve the system performance, including sub-6G channels, user positions, and 3D scene images obtained by cameras, etc. It should be noted that the conventional communication techniques can hardly take advantage of these out-of-band side-information due to the lack of tractable mathematical models. In fact, the development of techniques that utilize out-of-band side-information to improve the system performance has been an emerging research trend in DL based communications [17]–[19]. For example, [18] proposed a sub-6GHz channel information aided network for mmwave beam and blockage prediction, which could effectively reduce the overheads of both feedback

and beam training. In [19], a novel 3D scene based beam selection architecture was developed for mmwave communications by using the surrounding 3D scene of the cellular coverage as the input of networks.

Meanwhile, model aided DL has also made much progress recently. Instead of purely relying on training data, model aided DL benefits from the guidance of model information and therefore can achieve better performance [2]. For instance, [11] proposed an efficient DL based channel estimator by learning the linear model between least squares (LS) estimation and linear minimum mean square error (LMMSE) estimation. In [13], the authors proposed a model-driven DL based multiple-input multiple-output (MIMO) detector by unfolding a iterative algorithm, which can significantly outperform the corresponding traditional iterative detector.

Although a few DL based works tried to utilize multi-source sensing information (MSI), e.g., out-of-band side-information and model information, to improve the system performance, none of them has yet investigated how to integrate and comprehensively utilize these MSI in communication systems. From the viewpoint of machine learning, data from various sources are referred as multimodal sensory data, whereas data from one source are referred as data of a single modality. Communication systems naturally work with multimodal data and this clear advantage should not be squandered. Multimodal learning aims to build models that can fully exploit the constructive and complementary information lying in multimodal data, thus gaining performance advantages over methods that only use data of a single modality [22]. By combining DL architectures with multimodal learning methodologies, the concept of deep multimodal learning (DML) has been proposed in [23]. Thanks to the excellent flexibility of DL in extracting hierarchical features of data, DML offers several advantages over conventional multimodal learning, such as learning based feature extraction, implicit dimensionality reduction, and easily scalability in the modality number, etc [22]. The mainstream applications of DML include human action recognition, audio-visual speaker detection, and autonomous driving, etc [22]–[24]. For example, [24] jointly exploited two modalities, i.e., image and optical flow, for human action recognition, which could obtain higher recognition accuracy than only using image data.

This paper aims to develop a systematic framework on DML based wireless communications.

By using DML, the multimodal sensory data available in wireless communication systems can be fully exploited to provide constructive and complementary information for various tasks. The main contributions of this work can be summarized as following:

- We provide complete descriptions and analyses on the framework of DML. As opposed to [22], [23] that mainly studied DML in computer vision, speech, and natural language processing areas, this is the first work that explores how DML technologies can be applied to wireless communications to the best of the authors' knowledge, and we also provide some heuristic understandings.
- By investigating various modality combinations and fusion levels, we design several DML based architectures for channel prediction in massive MIMO systems as a case study. The design process presents a beneficial guidance on developing DML based communication technologies, while the proposed architectures can be easily extend to other communications problems like beam prediction, channel feedback, and resource allocation.
- Simulations based on ray-tracing software have been conducted and demonstrate that the proposed framework can effectively exploit the constructive and complementary information of multimodal sensory data in various scenarios.

The remainder of this paper is organized as follows. The motivation of exploring DML based wireless communications is given in Section II. The design choices of DML are presented in Section III. As a case study, Section IV proposed several DML based architectures for channel prediction in massive MIMO systems. Numerical results are provided in Section V, followed by our main conclusions in Section VI.

Notation: The bold letters denote vectors or matrices. The notation $\text{len}(\mathbf{z})$ denotes the length of the vector \mathbf{x} . The notations $(\cdot)^T$ and $(\cdot)^H$ respectively denote the transpose and the conjugate transpose of a matrix or a vector. The notation $\mathbb{C}^{m \times n}$ represents the $m \times n$ complex vector space. The notation $\|\mathbf{x}\|_2$ denotes the L_2 norm of \mathbf{x} . The notation \circ represents the composite mapping operation. The notations $\Re[\cdot]$ and $\Im[\cdot]$, respectively, denote the real and imaginary parts of matrices, vectors or scales. The notations $*$ and \otimes respectively represent the convolution operation and the matrix element-wise product. The notation $E[\cdot]$ represents the expectation with respect to all random variables within the brackets.

II. DML FOR WIRELESS COMMUNICATIONS

MSI in communication systems, including out-of-band side-information, model information, and other system information, is referred as multimodality. Information from one source is referred as one modality.

Multimodal sensory data of communication systems typically have varying *confidence levels*¹ when accomplishing different tasks. Take the beam selection at the base station (BS) as an example; the optimal beam vector can be obtained in three ways: (1) finding the best beam based on known downlink channels [26], (2) learning from 3D scene images [19], [20], and (3) extrapolating from sub-6G channels [18]. Among the three modalities, the downlink channels obviously have higher confidence level than both the 3D scene images and the sub-6G channels while the confidence level of the 3D scene images and the sub-6G channels depends on specific scenarios. Nevertheless, even when we have access to the modality with the highest confidence level, there may exist some modalities that could provide complementary information to further improve the performance or robustness of the single-modality based methods [27]. To better understand this, we can refer to the maximum ratio combining (MRC) [28], which is a widely adopted technology to obtain the combining gains of multi-antenna communication systems. MRC can benefit from the antennas with worse channels, which also provide a revelatory understanding about the gains brought by modalities with relatively lower confidence levels.

Meanwhile, multimodal sensory data usually have different dimensionality and structures. For example, in massive MIMO systems, the user position data could be a 3×1 real-valued vector, the received signals could be a much longer complex-valued vector, and the transmitted signals could be a high-dimensional complex-valued matrix. Therefore, it is important to design architectures that could fuse these modalities efficiently.

Few existing work so far has investigated how to integrate and fuse multimodal sensory data in the wireless communication problems. Motivated by this, we aim to develop a systematic framework on the DML based communications and illustrate the methodology by investigating the DML based channel prediction in massive MIMO systems.

¹The confidence level of one modality refers to the degree of the contribution or the reliability offered by the modality towards a certain task [25].

III. DESIGN CHOICES IN DML

The framework of DML consists of three core parts: selection, extraction and fusion. The selection process is to select appropriate models as well as effective modalities for a certain task. The extraction process is to extract information from involved modalities. The fusion process is to fuse the extracted information in order to obtain a fused representation of the multimodal sensory data. To embrace the performance advantages offered by DML, there are several design choices to be considered, including the selections of models, modalities, fusion levels, and fusion strategies, as will be illustrated in the following.

A. Model Selection

DL models can generally be divided into two categories: discriminative and generative models. Discriminative models aim to learn the mapping function from the inputs to the outputs, and are typically used to solve regression and classification tasks. In other words, given the input \mathbf{x} and the label \mathbf{y} , discriminative models learn the conditional probability $P(\mathbf{x}|\mathbf{y})$ by updating the model parameters. Since the majority of tasks in physical layer communications are to estimate \mathbf{y} based on \mathbf{x} , such as channel estimation [4], [6], [7], data detection [12], [13], [29], and beamforming [18]–[20], etc, existing DL techniques for physical layer communications mainly adopt discriminative models.

Generative models aim to learn the training data distribution that is required to generate new data with similar distributions. More specifically, generative models learn the joint probability $P(\mathbf{x}, \mathbf{y})$ in supervised learning problems, or learn the input data probability $P(\mathbf{x})$ in unsupervised or self-unsupervised learning problems. For DML problems, generative models are useful in the following three aspects: (1) Extracting features from different modalities, which are then used to perform discriminative tasks, i.e., regression and classification tasks. (2) Dealing with the situation of missing modalities during the test stage or lacking labeled data [30], [31]. (3) Providing good initialization points for discriminative models, such as DNNs [32].

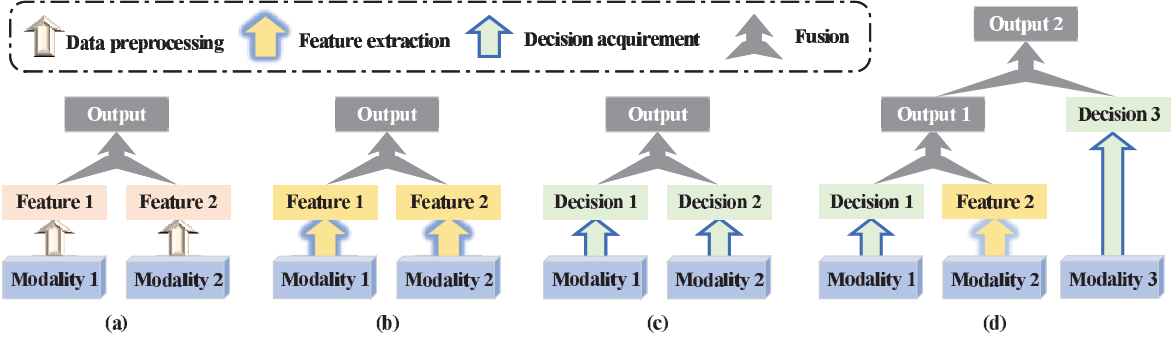


Fig. 1. Illustrations of various fusion levels for DML. (a) data fusion. (b) feature fusion. (c) decision fusion. (d) hybrid fusion.

B. Modality Selection

Different modalities may provide complementary information and have varying confidence levels for a certain multimodal learning task. Nevertheless, too much modalities may lead to information redundancy and an excessively complex fusion process. Therefore, it is worthwhile to select the optimal modalities by comprehensively considering the performance gain and the fusion complexity. In the area of computer vision and speech, the modality selection problem is generally considered as a tradeoff optimization [33]–[35]. For example, [33] proposed to select the optimal modalities based on the tradeoff between the feature dimensionality and the modality correlations. However, the authors did not take the confidence levels of modalities into account, which may miss modalities with high confidence levels. In [34], the authors utilize a dynamic programming approach to find the optimal subset of modalities based on the three-fold tradeoff between the performance gain, the overall confidence level of the selected subset, and the cost of the selected subset. In summary, [33]–[36] provided heuristic solutions for the modality selection problem in the context of multimedia data while there is hardly any literature studying modality selection for communication systems. A more direct way that is adopted in most of existing DML works is to manually select modalities by intuition and experiments.

C. Fusion Level Selection

In general, we can perform the modality fusion in four levels: data fusion, feature fusion, decision fusion, or hybrid fusion.

1) *Data fusion*: Data fusion is to concatenate the raw or preprocessed data of all the modalities into a single vector and then to learn a joint multimodal representation based on the concatenated vector during the fusion, as shown in Fig. 1 (a). Data fusion is simple to design and allows end-to-end training. An typical example of data fusion can refer to [4], where the received signals, the transmitted pilots, the pervious channels, and the LS estimates are directly concatenated as the inputs of networks to estimate channels in doubly selective fading scenarios. However, data fusion ignores the unique structure of different modalities, which may make it difficult to learn the complementary information among the modalities. In addition, simple concatenation of the multimodal sensory data leads to high-dimensional input vectors that may contain redundancies, especially when the number of modalities is large.

2) *Feature fusion*: Before we introduce the feature fusion, we first explain how to extract features from the raw or preprocessed data of one modality. The transform from the raw or preprocessed data to features is referred to as “feature extraction”. Feature extraction algorithms are either generative or discriminative, linear or nonlinear, such as principal component analysis [37], linear discriminative analysis [38], and Laplacian eigenmaps [39], etc. In recent few years, DNNs have been recognized as a popular technique to fuse modalities due to its excellent power and flexibility in extracting hierarchical features of the data. Specifically, each hidden layer of the network indeed represents a hierarchical features of the inputs. By changing the number of layers or choosing proper architecture, DNNs could extract features at various levels or with various dimensions. For example, [14] proposed a deep autoencoder architecture for channel feedback, where the dimension of the learnt compressed vector, i.e., the extracted feature that are used to reconstruct the original channel, can be adjusted according to the given compression ratio.

Now, we discuss the feature fusion. As illustrated in Fig. 1 (b), feature fusion is to fuse higher-level features into a single hidden layer and then to learn a joint multimodal representations for the output. By utilizing the extracted higher-level features, the model with feature fusion could learn higher-order correlations across modalities. Moreover, thanks to the flexibility of feature dimension reduction offered by DNNs, the feature fusion strategy may have more advantages than the data fusion strategy in learning multimodal representations [22].

3) *Decision fusion*: Before we introduce decision fusion, we first explain how to acquire a decision for one modality. The process of obtaining task results based on the modal data is referred to as “decision acquirement”. The decision acquirement can be realized by either DL based algorithms or conventional communication algorithms.

As shown in Fig. 1 (c), the decisions that are independently acquired by the involved modalities are fused to make a final decision, i.e., the output of the model. The disadvantage of decision fusion is that it cannot exploit the feature level correlation among modalities. The decision fusion strategy also has several advantages over the feature fusion strategy:

- When the involved modalities are completely uncorrelated or have very different dimensionality, it is much simpler and more reasonable to adopt decision fusion.
- Decision fusion makes it possible to adopt the most suitable algorithms to make decisions for each modality. In particular, for the modalities that can use accurate mathematical models to acquire the decision, conventional communication theories based algorithms would be more suitable than DL based algorithms.
- The fusion task would be more easier to implement since the decisions of different modalities usually have similar data representations.

4) *Hybrid fusion*: To embrace the merits of both the feature and the decision fusion strategies, hybrid fusion combines both feature and decision fusion in a unified framework. Fig. 1 (b) displays an example of hybrid fusion where the decisions and features of three modalities are fused at two different depths of the model. It should be emphasized that the decisions or features of multiple modalities can either be fused into a single layer or be fused gradually, i.e., modalities can be fused at different depths of the model. The choice at what depth to fuse which modalities is based on intuition and experiments. Take the channel estimation as an example. Given the three modalities, i.e., the pilots, the received signals, and the user position, we usually choose to first fuse the pilots and the received signals and then fuse the user position because the pilots and the received signals are highly correlated and the corresponding fusion should work well based on conventional communication theories. Besides, the gradual fusion strategy could also

avoid overlarge fusion vector, which partially solves the problem of dimensionality curse².

It should be mentioned that the fusion level selection depends on the specific problem, and therefore the superiority of the fusion level strategies should be investigated in a specific problem rather than in an absolute sense.

D. Fusion Strategy Selection

Various methods can be used to fuse different modalities, among which fixed-rule based fusion is the simplest one, including “max”, “min”, “average”, and “majority voting”, etc (see more rules in [41]). Besides, the linear weighted is also a common fusion strategy, where features or decisions of different modalities are combined with linear weights. One successful application of linear weighted is MRC, where the weights can be directly determined by channels. However, the linear weighted based modality fusion is not so simple like MRC. The greatest challenge lies in the determination of the weights for each modality, especially when the data dimension is high. To solve this problem, DNN based fusion has been proposed and gained growing attentions in these years [23], [24]. DNN based fusion could learn a nonlinear weighted mapping from the input to the output, and the weights could be adjusted by training with pre-acquired datasets instead of manual selection.

IV. CASE STUDY: DML FOR MASSIVE MIMO CHANNEL PREDICTION

In this section, we will first present the available modalities for channel prediction in massive MIMO systems. We will also give brief descriptions of the involved network architectures. Then, we will respectively discuss the architecture designs for the BS and the user, followed by detailed training steps of the proposed networks.

A. Available Modalities for Channel Prediction

Acquiring the channel knowledge plays a critical role in massive MIMO which is a promising technology for future wireless communication systems. This is mainly due to its high power

²The term “dimensionality curse” was first proposed in [40], which refers the phenomenon that when the data dimensionality increases, the dimension of feature space increases so fast that the available data become sparse and dissimilar in many ways. In this case, the amount of data required to support the data analysis often grows exponentially with the dimensionality.

efficiency and spectrum efficiency [42], [43]. In this work, we consider a massive MIMO system, where a BS is equipped with $M \gg 1$ antennas in the form of uniform linear array (ULA)³ and serves multiple single-antenna users. Note that the proposed approaches are applicable for uplink/downlink channel prediction in both TDD and FDD systems while we take the downlink channel prediction in FDD massive MIMO system as an typical example to illustrate the design and application of DML based channel prediction.

System model: To discuss the available modalities in FDD massive MIMO systems, we first present the mathematical model for the downlink transmission. Denote T_p as the pilot length. The received frequency domain signal of the u -th user on the k -th subcarrier is

$$\mathbf{r}[k] = \mathbf{h}_u^T(f_{D,k})\mathbf{s}[k] + \boldsymbol{\varepsilon}[k], \quad (1)$$

where $\mathbf{r}[k] \in \mathbb{C}^{1 \times T_p}$ is the received signal, $\mathbf{s}[k] \in \mathbb{C}^{M \times T_p}$ is the downlink pilot signal, $\boldsymbol{\varepsilon}[k]$ is the additive white Gaussian noise. Moreover, $\mathbf{h}_u(f_{D,k}) \in \mathbb{C}^{M \times 1}$ is the downlink channel that can be written as [44]

$$\mathbf{h}_u(f_{D,k}) = \sum_{p=1}^P \alpha_{u,p} e^{-j2\pi f_{D,k} \tau_{u,p} + j\phi_{u,p}} \mathbf{a}(\theta_{az}^{u,p}, \theta_{el}^{u,p}), \quad (2)$$

where P is the path number, $f_{D,k}$ is the frequency of the k -th downlink subcarrier, while $\alpha_{u,p}$, $\phi_{u,p}$, and $\tau_{u,p}$ are the attenuation, phase shift, and delay of the p -th path, respectively. In addition, $\mathbf{a}(\theta_{az}^{u,p}, \theta_{el}^{u,p})$ is the array manifold vector defined as

$$\mathbf{a}(\theta_{az}^{u,p}, \theta_{el}^{u,p}) = \left[1, e^{j\varpi \sin(\theta_{el}^{u,p}) \cos(\theta_{az}^{u,p})}, \dots, e^{j\varpi(M-1) \sin(\theta_{el}^{u,p}) \cos(\theta_{az}^{u,p})} \right]^T, \quad (3)$$

where $\varpi = 2\pi d f_{D,k} / c$, d is the antenna spacing, c is the speed of light, and $\{\theta_{az}^{u,p}, \theta_{el}^{u,p}\}$ is the {azimuth, elevation} angle of arrival. We employ the accurate 3D ray-tracing simulator Wireless InSite [45] to obtain the channel parameters in Eq. (2), i.e., $\{\alpha_{u,p}, \phi_{u,p}, \tau_{u,p}, \theta_{az}^{u,p}, \theta_{el}^{u,p}\}$. To simplify the notation, we drop the sub-carrier index k and the user index u in the rest of the paper, e.g., we replace $\mathbf{r}[k]$, $\mathbf{h}_u(f_{D,k})$, and $\mathbf{s}[k]$ with \mathbf{r} , $\mathbf{h}(f_D)$, and \mathbf{s} , respectively.

Available Modality: Available modalities in FDD massive MIMO system could be received

³We adopt the ULA model here for simpler illustration, nevertheless, the proposed approaches are not restricted to the specifical array shape, and therefore is applicable for array with arbitrary geometry.

signals, pilots, LS estimate, the downlink channels of previous coherent time periods, the uplink channel, the user location, and the partial downlink channel, as described in the following.

1) *Received signals and pilots*: Eq. (1) indeed reveals that there exists a mapping function from $\{\mathbf{r}, \mathbf{s}\}$ to $\mathbf{h}(f_D)$, which indicates that the received signals \mathbf{r} and the pilots \mathbf{s} are two modalities that could be jointly utilized to predict the downlink channel $\mathbf{h}(f_D)$.

2) *LS estimate*: When the number of pilots are sufficient (i.e., $T_p \geq M$), $\mathbf{h}(f_D)$ can be estimated by LS [46], i.e., $\hat{\mathbf{h}}_{\text{LS}}(f_D) = \mathbf{r}\mathbf{s}^H(\mathbf{s}\mathbf{s}^H)^{-1}$. In fact, the LS estimate $\hat{\mathbf{h}}_{\text{LS}}(f_D)$ can be regarded as one modality from model information.

3) *Previous downlink channels*: Denote the superscript (τ) as the index of coherent time periods. The downlink channels of previous coherent time periods, i.e., $\mathbf{h}^{(\tau-1)}(f_D), \mathbf{h}^{(\tau-2)}(f_D), \dots$, are referred as previous downlink channels, $\overleftarrow{\mathbf{h}}(f_D)$, for ease of exposition⁴. In practical systems, there exist unknown time correlations among channels that cannot be exploited by conventional channel estimation algorithms. Whereas such time correlations could be implicitly learned by DNNs and then be used to improve the prediction accuracy.

4) *User location*: The user location can be obtained by various techniques, such as the ultra-wideband, the global positioning system, and the wireless fidelity, etc. Many positioning works have revealed that there is a distinct link between the user's position and channels [47], [48]. Define the location-to-channel mapping as $\Phi_f : \{\mathbf{D}_{(x,y,z)}\} \rightarrow \{\mathbf{h}(f)\}$, where $\mathbf{D}_{(x,y,z)}$ is the 3D coordinate of the user, and f is the carrier frequency. Based on the universal approximation theorem [49] and the widely adopted assumption that Φ_f is a bijective deterministic mapping in massive MIMO systems [47], [48], we know that the mapping function Φ_f could be approximated arbitrarily well by a DNN under ideal conditions. Therefore, the modality of user location could be adopted to predict the downlink channel by using DNNs to learn the mapping Φ_{f_D} .

5) *Uplink channel*: Since uplink channels are easier to obtain than downlink channels in massive MIMO systems, many studies utilize uplink channels to aid the downlink channel prediction [9], [10], [50]. With the assumption that Φ_f is a bijective deterministic mapping,

⁴Since the downlink channel to be predicted and other modalities involved are all the data in the τ -th coherent time period, we have omitted the superscript (τ) of these realtime data for simplicity.

TABLE I
MODALITIES INVOLVED IN DOWNLINK CHANNEL PREDICTION

Modality	$\{r, s\}$	$\hat{h}_{LS}(f_D)$ [4], [11]	$\tilde{h}(f_D)$ [4], [5]	$D_{(x,y,z)}$	$h(f_U)$ [9], [10]	$\tilde{h}(f_D)$ [9], [51]
BS side	✓	×	✓	✓	✓	✓
User side	✓	✓	✓	✓	×	✓

the channel-to-location mapping Φ_f^{-1} exists and can be written as $\Phi_f^{-1} : \{h(f)\} \rightarrow \{D_{(x,y,z)}\}$.

Hence, the uplink-to-downlink mapping $\Psi_{U \rightarrow D}$ exists, and can be written as follows [9]:

$$\Psi_{U \rightarrow D} = \Phi_{f_D} \circ \Phi_{f_U}^{-1} : \{h(f_U)\} \rightarrow \{h(f_D)\}, \quad (4)$$

where f_U is the uplink frequency, and $\Phi_{f_D} \circ \Phi_{f_U}^{-1}$ represents the composite mapping related to Φ_{f_D} and $\Phi_{f_U}^{-1}$. Therefore, the modality of uplink channel could also be adopted to predict the downlink channel by using DNNs to learn the mapping $\Psi_{U \rightarrow D}$.

6) *Partial downlink channel*: Due to the high cost and power consumption of the radio-frequency chains, massive MIMO systems usually adopt hybrid analog and digital transceivers that are operated with switchers [21]. Therefore, given the limited transmission period and pilot length, only partial downlink channel can be obtained by the user and then be fed back to BS. Denote the partial downlink channel as $\tilde{h}(f_D)$ with $\text{len}(\tilde{h}(f_D)) < M$. Denote the vector consisting of unknown elements in $h(f_D)$ as $\hat{h}(f_D)$. Recalling Eq. (3) and Eq. (2), it is obvious that there exists a deterministic mapping from $\tilde{h}(f_D)$ to $\hat{h}(f_D)$, which can be written as $\Upsilon : \{\tilde{h}(f_D)\} \rightarrow \{\hat{h}(f_D)\}$. Therefore, we can predict the downlink channel by learning the mapping Υ .

In order to facilitate the analysis, we list the modalities for downlink channel prediction in Tab. I, where “✓” and “×” respectively represent the available and unavailable modalities for BS or the user. In particular, the modalities $\{r, s\}$ and $\tilde{h}(f_D)$ are available for BS because r and $\tilde{h}(f_D)$ could be fed back to the BS by the user. The modality $\hat{h}_{LS}(f_D)$ is obtained based on $\{r, s\}$. When the length of r is sufficiently long for the LS estimator, i.e., $T_p \geq M$, it would be more efficient to directly feed back the downlink channel rather than r to BS. Therefore, we set the modality $\hat{h}_{LS}(f_D)$ to be unavailable at BS. Tab. I also displays the existing works that utilize aforementioned modalities to predict channels. By trying and testing possible modality

combinations and feature level strategies, we can find the modalities with higher confidence levels and the modality combinations with better performance.

B. DNN Architectures

Based on the definition in Section III-A, the downlink channel prediction is a typical discriminative regression task. Since discriminative models are naturally suitable for feature extraction and decision acquirement in discriminative tasks, we choose discriminative models for downlink CSI prediction. The selections of both modalities and feature level strategies depends on specifical scenarios. Besides, due to the excellent learning capability of DNNs, we adopt DNN based fusion for channel prediction rather than fixed-rule based fusion.

Loss function: A DNN architecture consists of the input \mathbf{x} , the label \mathbf{y} , the output $\hat{\mathbf{y}}$, the network parameter Ω , the loss function $\text{Loss}(\Omega)$, a back-propagation learning algorithm, the activation functions and the network layers. Specifically, the network parameter Ω includes the weights and the biases of the network layers. The loss function adopted in this work is $\text{Loss}(\Omega) = \frac{1}{V} \sum_{v=0}^{V-1} \|\hat{\mathbf{y}}_v - \mathbf{y}_v\|_2^2$, where V is the batch size⁵, and the subscript v denotes the index of the v -th training sample. The back-propagation learning algorithm adopted in this work is the adaptive moment estimation (ADAM) algorithm [52]. In the off-line training stage, the network parameter Ω is updated by the ADAM algorithm to minimize the loss function $\text{Loss}(\Omega)$ on the training dataset. While in the on-line testing stage, Ω is fixed and the network could directly output the estimates of the labels in the testing dataset with a rather small error.

Activation function: The activation functions, including leaky rectified linear units (LeakyReLU)⁶, Sigmoid, and Tanh, apply element-wise nonlinear transformations to the outputs of the network layers. The functions LeakyReLU, Sigmoid, and Tanh can be respectively written as $\mathcal{F}_{\text{LR}}(\mathbf{x}) = \max\{\mathbf{x}, 0.2\mathbf{x}\}$, $\mathcal{F}_{\text{Sig}}(\mathbf{x}) = 1/(1 + e^{-\mathbf{x}})$, and $\mathcal{F}_{\text{Tan}}(\mathbf{x}) = (e^{\mathbf{x}} - e^{-\mathbf{x}})/(e^{\mathbf{x}} + e^{-\mathbf{x}})$.

Network layer: Fig. 2 depicts the structure of the network layers, including the dense, the convolution and the LSTM layers. As shown in Fig. 2 (a), the dense layer can be mathematically

⁵Batch size is the number of samples in one training batch.

⁶We adopt LeakyReLU instead of normal rectified linear units (ReLU) to avoid the “dead Relu” phenomenon [53].

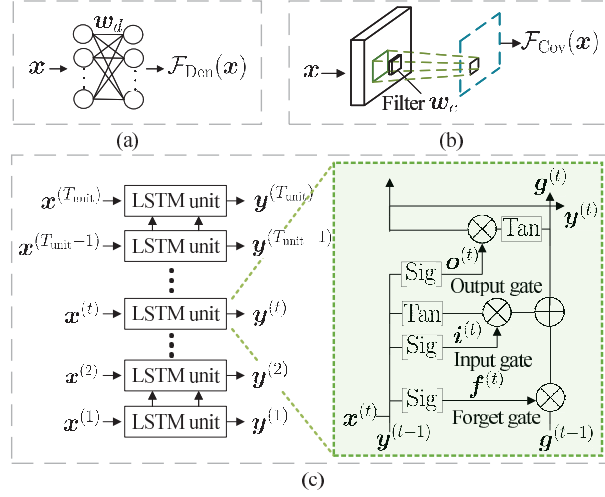


Fig. 2. Illustrations of the dense layer (a), the convolution layer (b), and the LSTM layer (c).

expressed as $\mathcal{F}_{\text{Den}}(x) = w_d x + b_d$, where w_d and b_d are the weight and the bias of the dense layer, respectively. Compared with the dense layer, the convolution layer is more powerful in learning the spatial features of the inputs. As illustrated in Fig. 2 (b), the convolution layer can be mathematically expressed as $\mathcal{F}_{\text{Cov}}(x) = w_c * x + b_c$, where w_c and b_c is the weight and the bias of the filter, respectively. Fig. 2 (c) depicts the structure of the LSTM layer, where each LSTM layer contains T_{unit} LSTM units. The output of the LSTM layer can be written as $\mathcal{F}_{\text{LSTM}}(x^{(1)}, \dots, x^{(T_{\text{unit}})}) = (y^{(1)}, \dots, y^{(T_{\text{unit}})})$. In the t -th ($1 \leq t \leq T_{\text{unit}}$) LSTM units, the relationships between the input $x^{(t)}$ and output $y^{(t)}$ can be expressed with the following equations:

$$i^{(t)} = \mathcal{F}_{\text{Sig}}(w_i [y^{(t-1)}, x^{(t)}] + b_i); \quad (5a)$$

$$f^{(t)} = \mathcal{F}_{\text{Sig}}(w_f [y^{(t-1)}, x^{(t)}] + b_f); \quad (5b)$$

$$o^{(t)} = \mathcal{F}_{\text{Sig}}(w_o [y^{(t-1)}, x^{(t)}] + b_o); \quad (5c)$$

$$g^{(t)} = f^{(t)} \otimes g^{(t-1)} + i^{(t)} \otimes \mathcal{F}_{\text{Tan}}(w_g [y^{(t-1)}, x^{(t)}] + b_g); \quad (5d)$$

$$y^{(t)} = o^{(t)} \otimes \mathcal{F}_{\text{Tan}}(g^{(t)}), \quad (5e)$$

where $\{w_i, w_f, w_o, w_g\}$ and $\{b_i, b_f, b_o, b_g\}$ are respectively the weights and the biases of the LSTM units, while $i^{(t)}$, $f^{(t)}$ and $o^{(t)}$ are respectively the input gate, the forget gate and output

gate. Moreover, $\mathbf{g}^{(t)}$ is the cell state of the t -th LSTM unit. Since the LSTM layer can effectively learn both the short-term and the long-term features through the memory cell and the gates, it has been recognized as a useful tool for time series related tasks.

C. Architecture Designs at the BS Side

Accurate downlink channels are crucial for BS to obtain high beamforming gains. Here we consider the downlink channel prediction problem under two different scenarios, i.e., feedback link is unavailable or is available. Before coming to specific architectures, we first present our main idea to design fusion architectures as follow:

- (i) Design and train elementary networks, i.e., the networks that adopt as few as possible modalities to independently predict downlink channels. In fact, all the modalities listed in Tab. I can independently predict downlink channels except the two modalities $\{\mathbf{r}, \mathbf{s}\}$ that should be jointly utilized to obtain downlink channels. Note that the performance of the elementary networks can be used to measure the confidence levels of the corresponding modalities.
- (ii) Design and train two-element based networks, i.e., the networks that fuse two elementary networks. the performance of the two-element based networks can be used to measure the complementarity of the corresponding modality combinations. When we design fusion architectures with multiple modalities, we will preferentially fuse the modality combinations with better performance and then fuse the modalities with higher confidence levels based on experiments and intuition [22], [54].

The idea is also applicable to the architecture designs at the user side as will be shown in the later section.

1) *Feedback link is unavailable:* In this scenario, available modalities are the previous downlink channels $\bar{\mathbf{h}}(f_D)$, the user location $\mathbf{D}_{(x,y,z)}$, and the uplink channel $\mathbf{h}(f_U)$. To investigate the confidence levels of the three modalities, we propose three networks, i.e., $\text{Net}\{\mathbf{H}\}$, $\text{Net}\{\mathbf{L}\}$, and $\text{Net}\{\mathbf{U}\}$ to respectively predict the downlink channel based on the previous downlink channels, the user location, and the uplink channel. Fig. 3 (a) illustrates the network structure of $\text{Net}\{\mathbf{H}\}$.

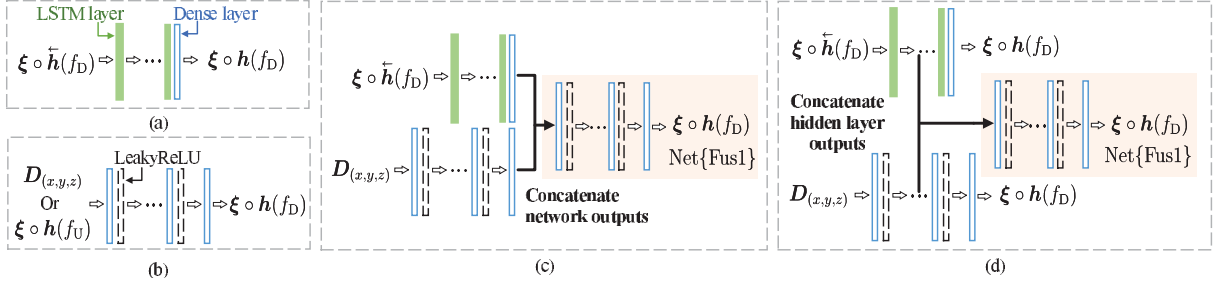


Fig. 3. The network structures of $\text{Net}\{\text{H}\}$ (a), $\text{Net}\{\text{L}\}$ (b), $\text{Net}\{\text{U}\}$ (b), $\text{Net}\{\text{H}, \text{L}\}_d$ (c), and $\text{Net}\{\text{H}, \text{L}\}_f$ (d).

The input of $\text{Net}\{\text{H}\}$ is $\xi \circ \bar{h}(f_D)$, where

$$\bar{h}(f_D) = [h^{(\tau-1)}(f_D), \dots, h^{(\tau-T_{\text{unit}})}(f_D)],$$

and ξ is the mapping between the complex and the real domains, i.e., $\xi : x \rightarrow (\Re(x^T), \Im(x^T))^T$. The label of $\text{Net}\{\text{H}\}$ is $\xi \circ h(f_D)$. The network $\text{Net}\{\text{H}\}$ is composed of several LSTM layers and one dense layer. Here we adopt the LSTM layer to predict the downlink channels for its superiority in time series data analyses. Besides, we add the dense layer after the last LSTM layer is to release the output of $\text{Net}\{\text{H}\}$ from the limited value range of the activation functions \mathcal{F}_{Tan} and \mathcal{F}_{Sig} , as indicated in Eq. (5e). Fig. 3 (b) shows the network structure of both $\text{Net}\{\text{L}\}$ and $\text{Net}\{\text{U}\}$, where the network is composed of several dense layers, and each dense layer except for the output layer is followed by the LeakyReLU function. Note that $\text{Net}\{\text{L}\}$ and $\text{Net}\{\text{U}\}$ have the common network structure and the same label $\xi \circ h(f_D)$, but they have different inputs and different hype-parameters, including the number of layers, the number of neurons in each layers, and the learning rates, etc.

To investigate the complementarities of the three modalities i.e., $\bar{h}(f_D)$, $D_{(x,y,z)}$, and $h(f_U)$, we first propose $\text{Net}\{\text{L}, \text{U}\}_d$, $\text{Net}\{\text{H}, \text{U}\}_d$, and $\text{Net}\{\text{H}, \text{L}\}_d$ to respectively fuse two of the three modalities at the decision levels. As shown in Fig. 3 (c), $\text{Net}\{\text{H}, \text{L}\}_d$ consists of $\text{Net}\{\text{H}\}$, $\text{Net}\{\text{L}\}$, and $\text{Net}\{\text{Fus1}\}$. The network $\text{Net}\{\text{Fus1}\}$, composed of several dense layers and LeakyReLU functions, concatenates the network outputs of $\text{Net}\{\text{H}\}$ and $\text{Net}\{\text{L}\}$ as its input vector. Note that the structures of $\text{Net}\{\text{L}, \text{U}\}_d$ and $\text{Net}\{\text{H}, \text{U}\}_d$ can be similarly obtained following the design of $\text{Net}\{\text{H}, \text{L}\}_d$. Therefore, we omit the descriptions of these networks for simplicity. Then, we

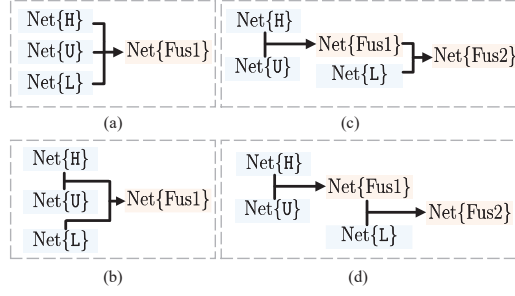


Fig. 4. The network structures of $\text{Net}\{H, L, U\}_d$ (a), $\text{Net}\{H, L, U\}_f$ (b), $\text{Net}\{H, L, U\}_{h1}$ (c), and $\text{Net}\{H, L, U\}_{h2}$ (d).

propose $\text{Net}\{L, U\}_f$, $\text{Net}\{H, U\}_f$, and $\text{Net}\{H, L\}_f$ to respectively fuse two of the three modalities at the feature levels. As shown in Fig. 3 (d), the main difference between $\text{Net}\{H, L\}_f$ and $\text{Net}\{H, L\}_d$ is that $\text{Net}\{H, L\}_f$ concatenates the hidden layer outputs rather than the network outputs of $\text{Net}\{H\}$ and $\text{Net}\{L\}$. Similarly, we omit the descriptions of $\text{Net}\{L, U\}_f$ and $\text{Net}\{H, U\}_f$ for simplicity. It should be explained that we do not consider data level fusion for $\bar{h}(f_D)$, $D_{(x,y,z)}$, and $h(f_U)$ since the three modalities have very different dimensions and data structures, which would result in inefficient data fusion.

Furthermore, we propose $\text{Net}\{H, L, U\}_d$ and $\text{Net}\{H, L, U\}_f$ to fuse all the three modalities at the decision and the feature levels, respectively. As illustrated in Fig. 4 (a) and Fig. 4 (b), $\text{Net}\{H, L, U\}_d$ and $\text{Net}\{H, L, U\}_f$ are both composed of $\text{Net}\{H\}$, $\text{Net}\{L\}$, $\text{Net}\{U\}$, and $\text{Net}\{Fus1\}$. The difference between $\text{Net}\{H, L, U\}_d$ and $\text{Net}\{H, L, U\}_f$ is that $\text{Net}\{H, L, U\}_f$ concatenates all the hidden layer outputs rather than the network outputs of $\text{Net}\{H\}$, $\text{Net}\{L\}$, and $\text{Net}\{U\}$. Moreover, we propose $\text{Net}\{H, L, U\}_{h1}$ and $\text{Net}\{H, L, U\}_{h2}$ to fuse all the three modalities at the hybrid levels. As depicted in Fig. 4 (c), $\text{Net}\{H, L, U\}_{h1}$ first uses $\text{Net}\{Fus1\}$ to fuse the hidden layer outputs of $\text{Net}\{H\}$ and $\text{Net}\{U\}$ and then uses $\text{Net}\{Fus2\}$ to fuse the network output of $\text{Net}\{Fus1\}$ and the hidden layer output of $\text{Net}\{L\}$. The only difference between $\text{Net}\{H, L, U\}_{h1}$ and $\text{Net}\{H, L, U\}_{h2}$ is that $\text{Net}\{H, L, U\}_{h1}$ fuses the network outputs of both $\text{Net}\{Fus1\}$ and $\text{Net}\{L\}$ while $\text{Net}\{H, L, U\}_{h2}$ fuses the hidden layer outputs of both $\text{Net}\{Fus1\}$ and $\text{Net}\{L\}$. It should be mentioned that we choose to first fuse $\text{Net}\{H\}$ and $\text{Net}\{U\}$ at the feature level because $\text{Net}\{H, U\}_f$ outperforms other proposed two-modality based networks, as will be shown in the later simulation section. This indicates that the fusion of $\bar{h}(f_D)$ and $h(f_U)$ provides stronger complementarity and therefore

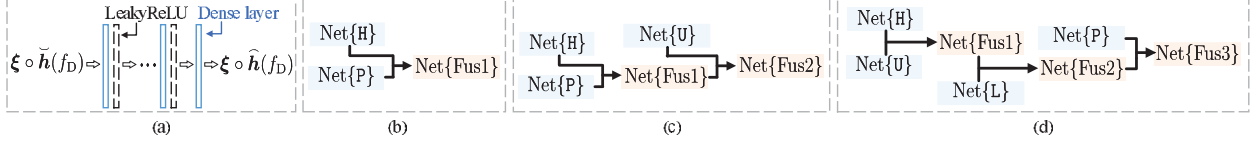


Fig. 5. The network structures of Net{P} (a), Net{P, H} (b), Net{P, H, U} (c), and Net{P, H, L, U} (d).

would be more suitable to be fused earlier. Note that the design and the testing for DML are not isolated but interoperable, which means that we need the testing results to guide the design of network. In other words, the excellent capability and flexibility of DML come at the cost of design complexity.

Remark 1: The channel prediction based on the three modalities, i.e., $\tilde{h}(f_D)$, $D_{(x,y,z)}$, and $h(f_U)$, can also be referred as the channel extrapolation across the time, space, and frequency domains. The three-modality based networks in Fig. 4 jointly exploit the complementarity of the time-space-frequency information to improve the performance of the channel extrapolation.

2) *Feedback link is available:* In this scenario, we need to investigate which modality would be more efficient to be fed back to BS under given feedback overhead. When the length of the vector to be fed back, denoted by T_{fb} , is greater than the number of BS antennas M , it is obvious that we should directly feed back the downlink channel rather than the received signal r . When T_{fb} is smaller than M , we respectively try various fusion networks for $\{r, s\}$ and $\tilde{h}(f_D)$ and then present the networks with the best performance in the following.

We first consider the case that $\tilde{h}(f_D)$ is fed back to BS. Obviously, the length of the vector $\hat{h}(f_D)$ is $M - T_{fb}$. As shown in Fig. 5 (a), we propose Net{P} to predict unknown $\hat{h}(f_D)$ based on the known $\tilde{h}(f_D)$, i.e., to learn the mapping Υ . The network structure of Net{P} is the same with Net{L} except that the input and the label of Net{P} are $\xi \circ \tilde{h}(f_D)$ and $\xi \circ \hat{h}(f_D)$, respectively. As shown in Fig. 5 (b), we propose Net{P, H} to fuse the network output of Net{P} and the hidden layer output of Net{H}. As presented in Fig. 5 (c), we propose Net{P, H, U} to fuse the network output of Net{P, H} and the hidden layer output of Net{U}. As illustrated in Fig. 5 (d), we propose Net{P, H, U, L} to fuse the network outputs of both $\text{Net}\{H, L, U\}_{h2}$ and Net{P}.

Then, we consider the case that r is fed back to BS. Since the length of the feedback vector

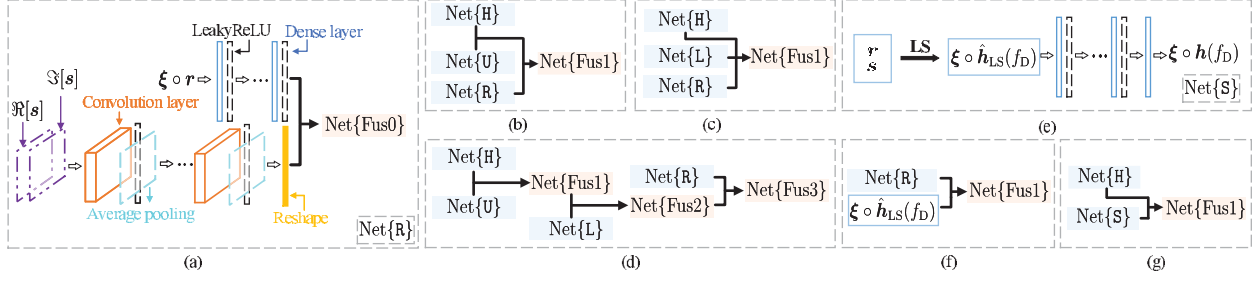


Fig. 6. The network structures of Net{R} (a), Net{R, H, U} (b), Net{R, H, L} (c), Net{R, H, L, U} (d), Net{S} (e), Net{S, R} (f), and Net{S, H} (g).

\mathbf{r} is smaller than M , i.e., $T_p = T_{fb} < M$, the LS estimator is not applicable due to the rank deficiency. However, it is feasible for DNNs to learn the mapping from $\{\mathbf{r}, \mathbf{s}\}$ to $\mathbf{h}(f_D)$, and thus we propose Net{R} to predict $\mathbf{h}(f_D)$ base on $\{\mathbf{r}, \mathbf{s}\}$. As shown in Fig. 6 (a), $\xi \circ \mathbf{r}$ is the input data of the first dense layer while $\Re[\mathbf{s}]$ and $\Im[\mathbf{s}]$ are concatenated at a new axis as the input data of the first convolution layer. Each convolution layer is followed by the LeakyReLU and the average pooling functions. The average pooling functions are added to down-sample the data stream and avoid overfitting [55]. After reshaping the output of the last convolution layer, we use Net{Fus0} to fuse the two data streams from the modalities \mathbf{r} and \mathbf{s} . The label of Net{R} is $\xi \circ \mathbf{h}(f_D)$. Moreover, we propose Net{R, H, U} to fuse the network output of Net{R} with the hidden layer outputs of both Net{H} and Net{U}, as depicted in Fig. 6 (b). We also propose Net{R, H, L} to fuse the hidden layer output of Net{H} with the network outputs of both Net{R} and Net{L}, as shown in Fig. 6 (c). As illustrated in Fig. 6 (d), we propose Net{R, H, L, U} to fuse the network outputs of both Net{H, L, U}_{h2} and Net{R}.

Remark 2: All the networks proposed in Section IV-C can be easily extended to other problems like beam prediction and antenna selection. Specifically, by replacing the labels of all these networks $\xi \circ \mathbf{h}(f_D)$ with the optimal beam vectors, the proposed architectures can handle the beam prediction at the BS side. Besides, the proposed architectures can deal with antenna selection by replacing the labels of all these networks with the optimal selection vectors. It is worth mentioning that the variant architectures for antenna selection do not require prefect downlink channels, which can significantly reduce the cost resulted from downlink channel prediction.

D. Architecture Designs at the User Side

We consider three different scenarios for downlink channel prediction at the user side, i.e., pilots being unavailable, insufficient or sufficient.

1) *Pilots are unavailable:* In this scenario, available modalities are the previous downlink channels $\tilde{\mathbf{h}}(f_D)$ and the user location $\mathbf{D}_{(x,y,z)}$. As described in Section IV-C1, we can use $\text{Net}\{\mathbf{H}\}$, $\text{Net}\{\mathbf{L}\}$, $\text{Net}\{\mathbf{H}, \mathbf{L}\}_d$ and $\text{Net}\{\mathbf{H}, \mathbf{L}\}_f$ to predict the downlink channels.

2) *Pilots are insufficient:* In this scenario, available modalities are $\tilde{\mathbf{h}}(f_D)$, $\mathbf{D}_{(x,y,z)}$, $\{\mathbf{r}, \mathbf{s}\}$, and $\tilde{\mathbf{h}}(f_D)$. As described in Section IV-C2, we can use $\text{Net}\{\mathbf{R}\}$, $\text{Net}\{\mathbf{P}, \mathbf{H}\}$ and $\text{Net}\{\mathbf{R}, \mathbf{H}, \mathbf{L}\}$ to predict the downlink channels.

3) *Pilots are sufficient:* When pilots are sufficient, the LS estimator can be used to estimate the downlink channel. Inspired by [4] and [11], we propose $\text{Net}\{\mathbf{S}\}$, consisting of several dense layers and LeakyReLU functions, to predict $\mathbf{h}(f_D)$ based on the LS estimate of downlink channel $\hat{\mathbf{h}}_{\text{LS}}(f_D)$, as illustrated in Fig. 6 (e). The input and label of $\text{Net}\{\mathbf{S}\}$ are $\boldsymbol{\xi} \circ \hat{\mathbf{h}}_{\text{LS}}(f_D)$ and $\boldsymbol{\xi} \circ \mathbf{h}(f_D)$, respectively. It should be emphasized that even when LS estimates have been obtained, the available modalities, i.e., $\tilde{\mathbf{h}}(f_D)$ and $\{\mathbf{r}, \mathbf{s}\}$, could also be adopted to enhance the accuracy. Moreover, we propose the $\text{Net}\{\mathbf{S}, \mathbf{R}\}$, as shown in Fig. 6 (f), where the network input of $\text{Net}\{\mathbf{S}\}$ and the network output of $\text{Net}\{\mathbf{R}\}$ are fused by $\text{Net}\{\text{Fus1}\}$. We also propose the $\text{Net}\{\mathbf{S}, \mathbf{H}\}$ to fuse the network output of $\text{Net}\{\mathbf{S}\}$ and the hidden layer output of $\text{Net}\{\mathbf{H}\}$, as displayed in Fig. 6 (g).

Remark 3: The networks $\text{Net}\{\mathbf{R}\}$, $\text{Net}\{\mathbf{R}, \mathbf{H}, \mathbf{L}\}$, and $\text{Net}\{\mathbf{S}, \mathbf{R}\}$ can be easily extended to data detection. One simple way inspired by [12] is to first divide the transmitted signals into pilots and data signals. Then, the pilots are fed to the network as depicted in Fig. 6 while the data signals are adopted as the training labels. In this way, we do not need to collect the downlink channels as training labels, which significantly reduce the cost for label collection.

E. Training Steps

The detailed training steps of all the proposed fusion networks are given as follows:

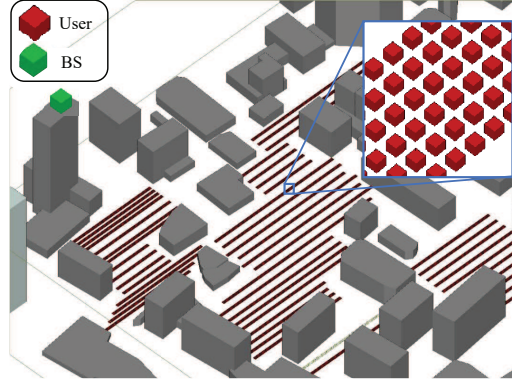


Fig. 7. A partial view of the ray-tracing scenario. The green little box represents the BS antennas. The red little box represents the possible location of the user antenna and the distance between adjacent red little boxes is 1 m. The red line is consistent with the y-axis. This ray-tracing scenario is constructed using the Remcom Wireless InSite [45].

- 1) Train the elementary networks, e.g., $\text{Net}\{H\}$, $\text{Net}\{L\}$, $\text{Net}\{U\}$, $\text{Net}\{P\}$, $\text{Net}\{R\}$ ⁷, and $\text{Net}\{S\}$, independently to minimize the loss between its output and the label $\xi \circ h(f_D)$ until their loss functions converge, and then fix these network parameters;
- 2) Train $\text{Net}\{\text{Fus1}\}$ to minimize the loss between its output and the label $\xi \circ h(f_D)$ until its loss function converges, and then fix its network parameters;
- 3) Following step 2), train $\text{Net}\{\text{Fus2}\}$ and $\text{Net}\{\text{Fus3}\}$ successively until their loss function converges and then fix their network parameters successively.

Obviously, the time and computation costs increase as the number of modalities increases. The balance between the cost and the performance should be considered in practical applications.

V. SIMULATION RESULTS

In this section, we will first present the simulation scenario and default network parameters. Then, the performance of the proposed networks will be evaluated and analyzed.

A. Simulation Setup

Dataset Generation: In the simulations, we consider the outdoor massive MIMO scenario that is constructed based on the accurate 3D ray-tracing simulator Wireless InSite [45]. Unlike

⁷ $\text{Net}\{R\}$ is trained in the end-to-end manner.

conventional statistical channel generation methods, the 3D ray-tracing simulator can capture the dependence of channels on the environment geometry/materials and transmitter/receiver locations, and therefore can provide more reliable datasets for training and testing. The scenario comprises one BS and massive randomly distributed user antennas and each BS is equipped with 64 antennas. The scenario covers an area of 500×500 square metres. A partial view of the ray-tracing scenario is illustrated in Fig. 7. The uplink and downlink frequencies are set to be 2.50 GHz and 2.62 GHz, respectively. Based on the environment setup, the 3D ray-tracing simulator outputs the uplink channel parameters, the downlink channel parameters, and the location $\mathbf{D}_{(x,y,z)}$ for each user. With these outputs, we can construct the training and testing datasets of all the modalities. Specifically, we can obtain $\mathbf{h}(f_U)$ and $\mathbf{h}(f_D)$ for each user by using Eq. (2) and the channel parameters from the 3D ray-tracing simulator. With Eq. (1), we can generate the pilots and the received signals $\{\mathbf{r}, \mathbf{s}\}$ based on $\mathbf{h}(f_D)$. Assuming that the previous downlink channels are the channels of the user at adjacent positions, and the users move along the y-axis. Then, $\tilde{\mathbf{h}}(f_D)$ can be obtained by collecting channels at adjacent T_{unit} positions. Partial downlink channel $\tilde{\mathbf{h}}(f_D)$ can be obtained by selecting M_{fb} elements out of $\mathbf{h}(f_D)$, and then the rest $M - M_{\text{fb}}$ elements constitute the vector $\hat{\mathbf{h}}(f_D)$. After obtaining all sample pairs, we randomly select 9000 samples from the sample pairs as the training dataset, and select 1000 samples from the rest of sample pairs as the testing dataset⁸. Since the perfect channels are not available in practical situation, unless otherwise specified, all the sample pairs in the datasets are estimated by the LMMSE algorithm [46] when the signal-to-noise ratio (SNR) is 25 dB and the pilot length is 64.

Adopted Neural Networks: Unless otherwise specified, the parameters of the proposed networks are given in Tab. II, where “LSTM: 256, 256” means that the hidden layers in $\text{Net}\{\mathbf{H}\}$ consists of two LSTM layers, and each hidden layer has 256 units. The numbers of units in the input and the output layers for all the proposed networks are consistent with the lengths of the input and the output data vectors, and thus are omitted in Tab. II. We choose the output of the middle hidden layer as the hidden layer output of the networks. The batch size V of all

⁸For more details about how to generate channels using Wireless InSite, please refer to the paper [44] and the codes [56].

TABLE II
DEFAULT PARAMETERS FOR THE PROPOSED NETWORKS

Network	Structure parameter	Learning rate
Net{H}	$T_u = 3$, LSTM: 256,256	5e-4
Net{L}	Dense: 256,256,256,256,256	1e-4
Net{U}	Dense: 256,256,256	1e-3
Net{P}	Dense: 256,256,256	5e-4
Net{R}	Dense: 256,128,128 Filter: 16, 32, 8 Kernel: (5, 5)	5e-4
Net{S}	Dense: 256	5e-4
Net{Fusi} i=0,1,2,3	Dense: 256,256	5e-4

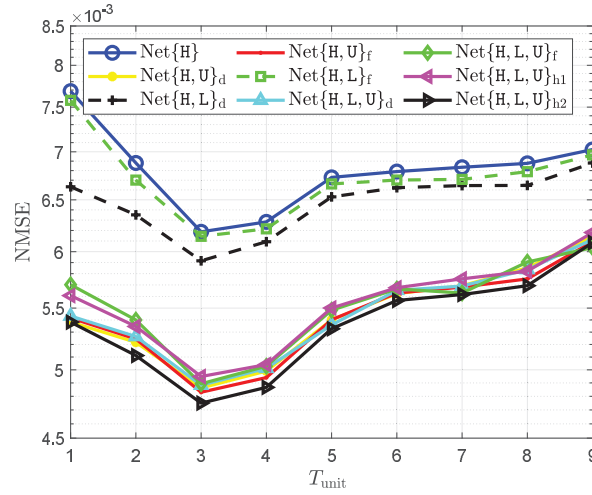


Fig. 8. The NMSE performance of previous downlink channel related networks versus T_{unit} .

proposed networks is 128. Let $\hat{\mathbf{h}}_D = \boldsymbol{\xi}^{-1} \circ \hat{\mathbf{y}}$ and $\mathbf{h}_D = \boldsymbol{\xi}^{-1} \circ \mathbf{y}$ represent the estimated and the true downlink channels, respectively⁹. Normalized mean-squared-error (NMSE) is used to measure the prediction accuracy, which is defined as $\text{NMSE} = E \left[\left\| \mathbf{h}_D - \hat{\mathbf{h}}_D \right\|_2^2 / \left\| \mathbf{h}_D \right\|_2^2 \right]$.

B. BS Side

Fig. 8 displays the NMSE performance of the previous downlink channel related networks versus T_{unit} . A larger T_{unit} means that Net{H} would learn time correlation of downlink channels from previous downlink channels in longer time periods. It can be observed that the performance of all these networks first improves and then degrades as T_{unit} increases, which indicates that the

⁹The notation $\boldsymbol{\xi}^{-1}$ denotes the inverse mapping of $\boldsymbol{\xi}$ that is given as $\boldsymbol{\xi}^{-1} : (\Re(z^T), \Im(z^T))^T \rightarrow z$.

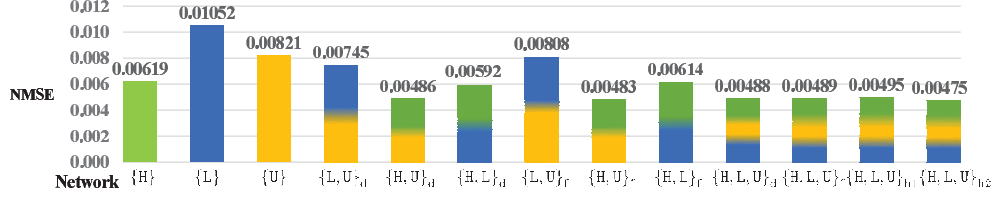


Fig. 9. The NMSE performance of the networks that are applicable to BS without feedback link.

channels within 3 time periods have positive contributions to the downlink channel prediction while the channels beyond 3 time periods have negative impact on the downlink channel prediction. Furthermore, $\text{Net}\{H\}$ always performs worse than other fusion networks, and $\text{Net}\{H, L, U\}_{h2}$ outperforms other networks regardless of the value of T_{unit} in the considered setup. This implies that the modalities $D_{(x,y,z)}$ and $h(f_U)$ do provide complementary information for $\text{Net}\{H\}$. We will set T_{unit} to be 3 for better performance in the following simulations.

Fig. 9 shows the NMSE performance of all networks that are applicable to BS without feedback link, as discussed in Section IV-C1. As shown in Fig. 9, all the two-modalities fused networks outperform the corresponding two single-modality networks, which implies that any two of the three modalities, i.e., $\bar{h}(f_D)$, $D_{(x,y,z)}$ and $h(f_U)$, can provide complementary information, thus enhancing the prediction accuracy. In particular, although $\text{Net}\{L\}$ has worse performance than both $\text{Net}\{H\}$ and $\text{Net}\{U\}$, the four two-modalities fused networks, i.e., $\text{Net}\{H, L\}_d$, $\text{Net}\{H, L\}_f$, $\text{Net}\{L, U\}_d$, and $\text{Net}\{L, U\}_f$, all have better performance than both $\text{Net}\{H\}$ and $\text{Net}\{U\}$. Besides, we notice that $\text{Net}\{H, U\}_f$ has the best performance among two-modalities fused networks and $\text{Net}\{H, L, U\}_{h2}$ outperforms other three-modalities fused networks. In fact, the structure of $\text{Net}\{H, L, U\}_{h2}$ is inspired by that of $\text{Net}\{H, U\}_f$. More specifically, since $\text{Net}\{H, U\}_f$ outperforms other two-modalities fused networks, we choose to preferentially fuse $\bar{h}(f_D)$ and $h(f_U)$ at the feature level.

Fig. 10 compares the NMSE performance of all the networks that are applicable to BS with feedback link, as discussed in Section IV-C2. As shown in Fig. 10, the performance of all the proposed networks improves when the feedback length T_{fb} increases. As indicated in the first enlarge picture, it would be better to feed the partial downlink channel back to BS when T_{fb} is greater than 48, otherwise it would be better to feed the received signal back to BS. Furthermore,

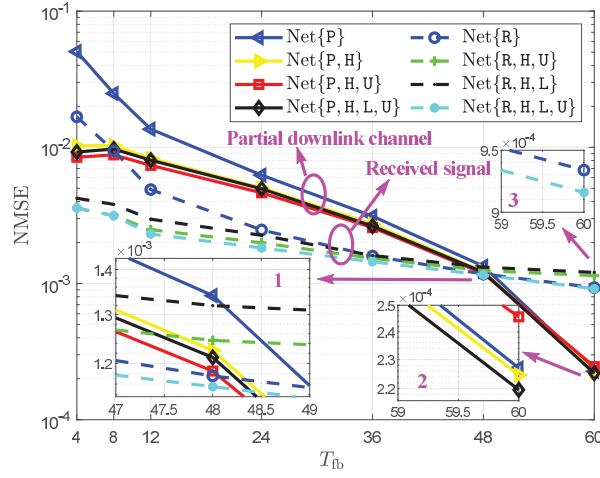


Fig. 10. The NMSE performance of all the networks that are applicable to BS with feedback link. The networks are trained separately for each value of T_{fb} .

it can be observed from the second enlarge picture that $\text{Net}\{P, H\}$ and $\text{Net}\{P, H, L, U\}$ consistently outperform $\text{Net}\{P\}$ while the gaps between the three networks all degrade as T_{fb} increases. This indicates that when we choose to feed partial downlink channel back, i.e., $T_{fb} \leq 48$, we can adopt $\text{Net}\{P\}$ instead of other $\tilde{\mathbf{h}}(f_D)$ related fusion networks to reduce the training cost, since the gaps between them are negligible. Moreover, as shown in the third enlarge picture, $\text{Net}\{R, H, L, U\}$ consistently outperforms $\text{Net}\{R\}$, $\text{Net}\{R, H, U\}$, and $\text{Net}\{R, H, L\}$ while the gap between $\text{Net}\{R, H, L, U\}$ and $\text{Net}\{R\}$ becomes negligible when T_{fb} is larger than 36. This indicates that we can adopt $\text{Net}\{R, H, L, U\}$ for better prediction accuracy when T_{fb} is smaller than 36 and adopt $\text{Net}\{R\}$ for lower training cost when T_{fb} is greater than 36 and less than 48.

C. User Side

Fig. 11 displays the NMSE performance of LS, $\text{Net}\{R\}$, $\text{Net}\{S\}$, $\text{Net}\{S, R\}$, and $\text{Net}\{S, H\}$ versus the pilot length T_p , where SNR is 30 dB. As shown in Fig. 11, $\text{Net}\{S, H\}$ has worse performance than $\text{Net}\{S\}$, which means $\tilde{\mathbf{h}}(f_D)$ cannot provide complementary information for $\text{Net}\{S\}$ when SNR is high and the number of pilots is sufficient, i.e., $T_p > 64$. In other words, when the number of pilots is sufficient and SNR is high, the modalities $\{r, s\}$ have the highest confidence level and other modalities can hardly provide complementary information to improve the performance. Moreover, the LS estimator outperforms $\text{Net}\{R\}$ when T_p is greater than

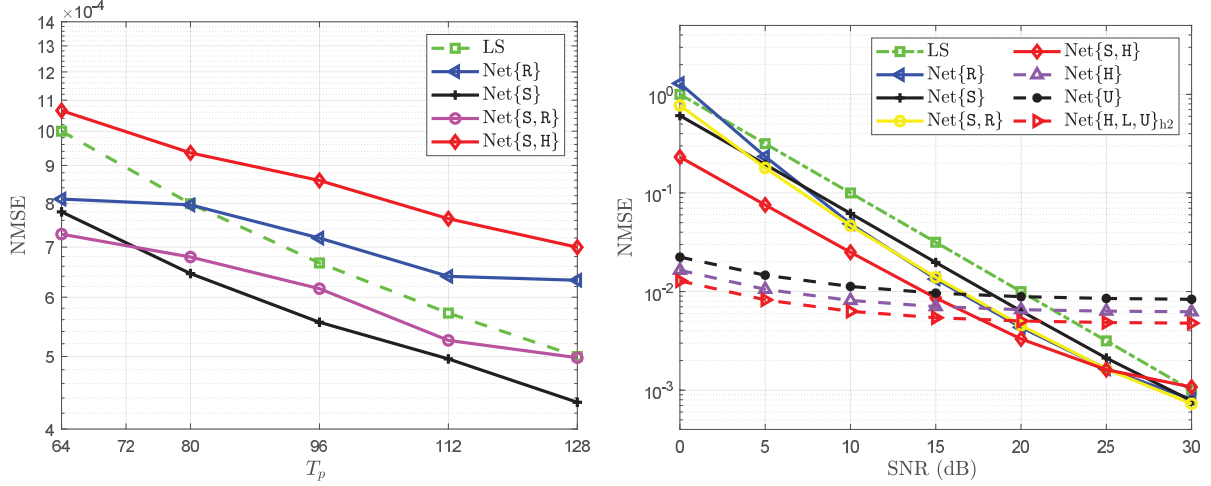


Fig. 11. The NMSE performance of LS, Net{R}, Net{S}, Fig. 12. The NMSE performance of the proposed networks Net{S, R}, and Net{S, H} versus the pilot length T_p . The versus SNR, where T_p is 64. The networks are trained separately for each value of T_p . separately for each value of SNR.

80, which implies that model-based methods would gain more advantages than network-based methods as T_p increases. Furthermore, Net{S, R} outperforms Net{S} when T_p is smaller than 72, which means networks can learn extra features from $\{r, s\}$ to improve the performance when T_p is smaller than 72, while when T_p is greater than 72, $\{r, s\}$ would provide redundant information to the network and result in worse performance. To obtain better performance at the user side, we can choose Net{S, R} when T_p is in $[64, 72]$ and choose Net{S} when T_p is greater than 72.

D. Impairments in Practical Applications

To collect off-line training samples, we can obtain extremely accurate channels by increasing SNR and the pilot length. However, in the on-line testing stage, low SNRs would impair the prediction accuracy of the proposed networks. Therefore, we investigate the impact of various SNRs on the performance of LS, Net{R}, Net{S}, Net{S, R}, Net{S, H}, Net{H}, Net{U}, and Net{H, L, U}_{h2}, where T_p is 64. Fig. 12 shows the performance of these networks versus the SNR in the on-line testing stage. Notice that the performance of Net{H}, Net{U}, and Net{H, L, U}_{h2} becomes saturated when SNR is higher than 15 dB, which means that the estimation errors of the input channels would not impact the performance of the three networks when SNR is higher

than 15 dB. As indicated in Fig. 12, $\text{Net}\{H, L, U\}_{h2}$ outperforms all other networks when SNR is lower than 17 dB while $\text{Net}\{S, H\}$ outperforms $\text{Net}\{H, L, U\}_{h2}$ when SNR is higher than 17 dB. This is because that the estimation based on pilots and received signals highly relies on SNR while the prediction based on $\hat{h}(f_D)$, $D_{(x,y,z)}$, and $h(f_U)$ are more robust over SNR. To obtain a better prediction accuracy, BS should choose $\text{Net}\{H, L, U\}_{h2}$ when SNR is lower than 17 dB and use feedback link to obtain the downlink channel estimated by the user when SNR is higher than 17 dB. Furthermore, $\text{Net}\{H\}$ outperforms $\text{Net}\{S, H\}$ when SNR is lower than 16 dB while $\text{Net}\{S, H\}$ outperforms $\text{Net}\{H\}$ when SNR is higher than 16 dB. Notice that both $\text{Net}\{S, R\}$ and $\text{Net}\{R\}$ outperform $\text{Net}\{S, H\}$ when SNR is greater than 25 dB. This implies that the user should choose $\text{Net}\{H\}$ when SNR is lower than 16 dB, choose $\text{Net}\{S, H\}$ when SNR is in $[16, 25]$ dB, and choose $\text{Net}\{R\}$ when SNR is greater than 25 dB.

Discussion: As mentioned in Section IV-C1, the design and the testing for DML are interoperable, which is a typical characteristic of data-driven techniques. On the contrary, conventional communications are model-driven, where the algorithm designs rely on prerequisite models and their performance is completely predictable and explicable. In this paper, we have provided a heuristic framework for DML based communications, and the theoretical guidance on the framework will be left for future work.

VI. CONCLUSION

In this paper, we introduced DML into wireless communications to fully exploit the MSI in communication systems such that the system performance could be improved. We provided complete descriptions and heuristic analyses of the design choices in DML based wireless communications. We also proposed several efficient DML based architectures for channel prediction as a case study. Simulation results have shown that DML based architectures exhibit significant advantages over one modality based architectures under most cases, which also demonstrate that the proposed framework can effectively exploit the constructive and complementary information of multimodal sensory data to assist the current wireless communications.

REFERENCES

- [1] T. Wang, C. Wen, H. Wang, F. Gao, T. Jiang, and S. Jin, "Deep learning for wireless physical layer: Opportunities and challenges," *China Commun.*, vol. 14, no. 11, pp. 92–111, Nov. 2017.

- [2] H. He, S. Jin, C. Wen, F. Gao, G. Y. Li, and Z. Xu, "Model-driven deep learning for physical layer communications," *IEEE Wireless Commun.*, vol. 26, no. 5, pp. 77–83, Oct. 2019.
- [3] Z. Qin, H. Ye, G. Y. Li, and B. F. Juang, "Deep learning in physical layer communications," *IEEE Wireless Commun.*, vol. 26, no. 2, pp. 93–99, Apr. 2019.
- [4] Y. Yang, F. Gao, X. Ma, and S. Zhang, "Deep learning-based channel estimation for doubly selective fading channels," *IEEE Access*, vol. 7, pp. 36579–36589, Mar. 2019.
- [5] X. Ma, H. Ye, and Y. Li, "Learning assisted estimation for time-varying channels," in *Proc. 15th Int. Symp. Wireless Commun. Systems (ISWCS)*, Lisbon, Portugal, Aug. 2018, pp. 1–5.
- [6] H. He, C. Wen, S. Jin, and G. Y. Li, "Deep learning-based channel estimation for beamspace mmwave massive MIMO systems," *IEEE Wireless Commun. Lett.*, vol. 7, no. 5, pp. 852–855, Oct. 2018.
- [7] P. Dong, H. Zhang, G. Y. Li, I. S. Gaspar, and N. NaderiAlizadeh, "Deep CNN-based channel estimation for mmwave massive MIMO systems," *IEEE J. Sel. Topics Signal Process.*, vol. 13, no. 5, pp. 989–1000, Sept. 2019.
- [8] Y. Yang, F. Gao, C. Qian, and G. Liao, "Model-aided deep neural network for source number detection," *IEEE Signal Process. Lett.*, vol. 27, pp. 91–95, 2020.
- [9] M. Alrabeiah and A. Alkhateeb, "Deep learning for TDD and FDD massive MIMO: Mapping channels in space and frequency," in *Proc. 53rd Asilomar Conf. Signals, Systems, Computers*, California, USA, 2019, pp. 1465–1470.
- [10] Y. Yang, F. Gao, G. Y. Li, and M. Jian, "Deep learning based downlink channel prediction for FDD massive MIMO system," *IEEE Commun. Lett.*, vol. 23, no. 11, pp. 1994–1998, Nov. 2019.
- [11] X. Gao, S. Jin, C. Wen, and G. Y. Li, "Comnet: Combination of deep learning and expert knowledge in OFDM receivers," *IEEE Commun. Lett.*, vol. 22, no. 12, pp. 2627–2630, Oct. 2018.
- [12] H. Ye, G. Y. Li, and B. Juang, "Power of deep learning for channel estimation and signal detection in OFDM systems," *IEEE Wireless Commun. Lett.*, vol. 7, no. 1, pp. 114–117, Feb. 2018.
- [13] H. He, C. Wen, S. Jin, and G. Y. Li, "Model-driven deep learning for MIMO detection," *IEEE Trans. Signal Process.*, vol. 68, pp. 1702–1715, Feb. 2020.
- [14] C. Wen, W. Shih, and S. Jin, "Deep learning for massive MIMO CSI feedback," *IEEE Wireless Commun. Lett.*, vol. 7, no. 5, pp. 748–751, Oct. 2018.
- [15] T. Wang, C. Wen, S. Jin, and G. Y. Li, "Deep learning-based CSI feedback approach for time-varying massive MIMO channels," *IEEE Wireless Commun. Lett.*, vol. 8, no. 2, pp. 416–419, Apr. 2019.
- [16] J. Guo, C. Wen, S. Jin, and G. Y. Li, "Convolutional neural network based multiple-rate compressive sensing for massive MIMO CSI feedback: Design, simulation, and analysis," *IEEE Trans. Wireless Commun.*, vol. 19, no. 4, pp. 2827–2840, Apr. 2020.
- [17] K. Ma, P. Zhao, and Z. wang, "Deep learning assisted beam prediction using out-of-band information," in *Proc. IEEE 91st Vehicular Technol. Conf.*, Antwerp, Belgium, May 2020, pp. 1–5.
- [18] M. Alrabeiah and A. Alkhateeb, "Deep learning for mmwave beam and blockage prediction using sub-6GHz channels," *arXiv preprint arXiv:1910.02900*, 2019.
- [19] W. Xu, F. Gao, S. Jin, and A. Alkhateeb, "3D scene based beam selection for mmwave communications," *arXiv preprint arXiv:1911.08409*, 2019.
- [20] M. Alrabeiah, A. Hredzak, Z. Liu, and A. Alkhateeb, "ViWi: A deep learning dataset framework for vision-aided wireless communications," *arXiv preprint arXiv:1911.06257*, 2019.
- [21] X. Li and A. Alkhateeb, "Deep learning for direct hybrid precoding in millimeter wave massive MIMO systems," in *53rd Asilomar Conf. Signals, Systems, Computers*, California, USA, Nov. 2019, pp. 800–805.
- [22] D. Ramachandram and G. W. Taylor, "Deep multimodal learning: A survey on recent advances and trends," *IEEE Signal Process. Mag.*, vol. 34, no. 6, pp. 96–108, 2017.
- [23] J. Ngiam, A. Khosla, M. Kim, J. Nam, H. Lee, and A. Y. Ng, "Multimodal deep learning," in *Proc. 28th Int. Conf. Int. Conf. Machine Learning (ICML)*, Madison, WI, USA, Jun. 2011, pp. 689–696, Omnipress.
- [24] C. Feichtenhofer, A. Pinz, and A. Zisserman, "Convolutional two-stream network fusion for video action recognition," in *Proc. IEEE Conf. Computer Vision Pattern Recognition (CVPR)*, Las Vegas, USA, Jun. 2016, pp. 1933–1941.
- [25] P. Atrey, M. Hossain, A. El Saddik, and M. Kankanhalli, "Multimodal fusion for multimedia analysis: A survey," *Multimedia Syst.*, vol. 16, no. 6, pp. 345–379, Nov. 2010.
- [26] F. Zhu, F. Gao, H. Lin, S. Jin, J. Zhao, and G. Qian, "Robust beamforming for physical layer security in BDMA massive MIMO," *IEEE J. Selected Areas Commun.*, vol. 36, no. 4, pp. 775–787, Apr. 2018.

- [27] G. Potamianos, C. Neti, G. Gravier, A. Garg, and A. W. Senior, "Recent advances in the automatic recognition of audiovisual speech," *Proc. IEEE*, vol. 91, no. 9, pp. 1306–1326, Sept. 2003.
- [28] D. Tse and P. Viswanath, *Fundamentals of wireless communication*, Cambridge university press, 2005.
- [29] Z. Jia, W. Cheng, and H. Zhang, "A partial learning-based detection scheme for massive MIMO," *IEEE Wireless Commun. Lett.*, vol. 8, no. 4, pp. 1137–1140, Aug. 2019.
- [30] N. Srivastava and R. Salakhutdinov, "Learning representations for multimodal data with deep belief nets," in *Proc. Int. conf. machine learning workshop*, 2012, vol. 79.
- [31] Y. Huang, W. Wang, and L. Wang, "Unconstrained multimodal multi-label learning," *IEEE Trans. Multimedia*, vol. 17, no. 11, pp. 1923–1935, 2015.
- [32] G. Hinton, L. Deng, D. Yu, G. E. Dahl, A. Mohamed, N. Jaitly, A. Senior, V. Vanhoucke, P. Nguyen, T. N. Sainath, and B. Kingsbury, "Deep neural networks for acoustic modeling in speech recognition: The shared views of four research groups," *IEEE Signal Process. Mag.*, vol. 29, no. 6, pp. 82–97, Oct 2012.
- [33] Y. Wu, E. Chang, K. Chang, and J. Smith, "Optimal multimodal fusion for multimedia data analysis," in *Proc. 12th Annual ACM Int. Conf. Multimedia*, New York, NY, USA, 2004, pp. 572–579, Association for Computing Machinery.
- [34] P. Atrey, M. Kankanhalli, and J. Oommen, "Goal-oriented optimal subset selection of correlated multimedia streams," *ACM Trans. Multimedia Comput. Commun. Appl.*, vol. 3, no. 1, pp. 2, Feb 2007.
- [35] S. Lemmelä, "Selecting optimal modalities for multimodal interaction in mobile and pervasive environments," in *Proc. Improved Mobile User Experience workshop*, May 2008.
- [36] M. S. Kankanhalli, J. Wang, and R. Jain, "Experiential sampling in multimedia systems," *IEEE Trans. Multimedia*, vol. 8, no. 5, pp. 937–946, Sept. 2006.
- [37] U. Demšar, P. Harris, C. Brunson, A. Fotheringham, and S. McLoone, "Principal component analysis on spatial data: an overview," *Annals Association American Geographers*, vol. 103, no. 1, pp. 106–128, 2013.
- [38] A. Sharma and K. Paliwal, "Linear discriminant analysis for the small sample size problem: an overview," *Int. J. Machine Learning Cybernetics*, vol. 6, no. 3, pp. 443–454, 2015.
- [39] M. Belkin and P. Niyogi, "Laplacian eigenmaps for dimensionality reduction and data representation," *Neural Computation*, vol. 15, no. 6, pp. 1373–1396, 2003.
- [40] R. Bellman, "Dynamic programming," 1957.
- [41] J. Kittler, M. Hatef, R. P. W. Duin, and J. Matas, "On combining classifiers," *IEEE Trans. Pattern Analysis Machine Intelligence*, vol. 20, no. 3, pp. 226–239, Mar. 1998.
- [42] B. Wang, F. Gao, S. Jin, H. Lin, and G. Y. Li, "Spatial- and frequency-wideband effects in millimeter-wave massive MIMO systems," *IEEE Trans. Signal Process.*, vol. 66, no. 13, pp. 3393–3406, Jul. 2018.
- [43] H. Xie, F. Gao, S. Zhang, and S. Jin, "A unified transmission strategy for TDD/FDD massive MIMO systems with spatial basis expansion model," *IEEE Trans. Vehicular Technol.*, vol. 66, no. 4, pp. 3170–3184, Apr. 2017.
- [44] A. Alkhateeb, "DeepMIMO: A generic deep learning dataset for millimeter wave and massive MIMO applications," in *Proc. Inf. Theory and Applications Workshop (ITA)*, San Diego, CA, Feb. 2019, pp. 1–8.
- [45] "Remcom wireless insite," <https://www.remcom.com/wireless-insite-em-propagation-software>.
- [46] M. Biguesh and A. B. Gershman, "Training-based MIMO channel estimation: a study of estimator tradeoffs and optimal training signals," *IEEE Trans. Signal Process.*, vol. 54, no. 3, pp. 884–893, Mar. 2006.
- [47] C. Studer, S. Medjkouh, E. Gonultas, T. Goldstein, and O. Tirkkonen, "Channel charting: Locating users within the radio environment using channel state information," *IEEE Access*, vol. 6, pp. 47682–47698, Aug. 2018.
- [48] J. Vieira, E. Leitingner, M. Sarajlic, X. Li, and F. Tufvesson, "Deep convolutional neural networks for massive MIMO fingerprint-based positioning," in *Proc. IEEE 28th Annual Int. Symposium Personal, Indoor, Mobile Radio Communications (PIMRC)*, Montreal, Canada, Oct. 2017, pp. 1–6.
- [49] K. Hornik, M. Stinchcombe, and H. White, "Multilayer feedforward networks are universal approximators," *Neural netw.*, vol. 2, no. 5, pp. 359–366, 1989.
- [50] H. Xie, F. Gao, S. Jin, J. Fang, and Y. Liang, "Channel estimation for TDD/FDD massive MIMO systems with channel covariance computing," *IEEE Trans. Wireless Commun.*, vol. 17, no. 6, pp. 4206–4218, Jun. 2018.
- [51] P. Dong, H. Zhang, and G. Y. Li, "Machine learning prediction based CSI acquisition for FDD massive MIMO downlink," in *Proc. IEEE Global Commun. Conf. (GLOBECOM)*, Abu Dhabi, United Arab Emirates, Dec. 2018, pp. 1–6.
- [52] D. Kingma and J. Ba, "Adam: A method for stochastic optimization," *arXiv preprint arXiv:1412.6980*, 2014.

- [53] A. Maas, A. Hannun, and A. Ng, “Rectifier nonlinearities improve neural network acoustic models,” in *Proc. 30th Int. Conf. Machine Learning (ICML)*, Atlanta, Georgia, USA, 2013, vol. 30, p. 3.
- [54] N. Neverova, C. Wolf, G. Taylor, and F. Nebout, “Moddrop: Adaptive multi-modal gesture recognition,” *IEEE Trans. Pattern Analysis Machine Intelligence*, vol. 38, no. 8, pp. 1692–1706, Jul. 2016.
- [55] M. Sun, Z. Song, X. Jiang, J. Pan, and Y. Pang, “Learning pooling for convolutional neural network,” *Neurocomputing*, vol. 224, pp. 96–104, Feb. 2017.
- [56] “Codes,” [Online]. Available: <https://github.com/yangyuwenyang/Codes-for-DML>.